Received: 21 June 2021 | Revised: 17 November 2021 | Accepted: 24 November 2021

DOI: 10.1002/qj.4223

Quarterly Journal of the Royal Meteorological Society RMetS

RESEARCH ARTICLE

Cold pools over the Netherlands: A statistical study from tower and radar observations

Irene L. Kruse[1,2] | **Jan O. Haerter**[1,2,3] | **Bettina Meyer**[1]

[1]Niels Bohr Institute, Copenhagen University, Copenhagen, Denmark

[2]Complexity and Climate, Leibniz Center for Tropical Marine Research, Bremen, Germany

[3]Physics and Earth Sciences, Jacobs University Bremen, Bremen, Germany

Correspondence
I. L. Kruse, Niels Bohr Institute, Copenhagen University, Blegdamsvej 17, 2100 Copenhagen, Denmark; Leibniz Centre for Tropical Marine Research, Fahrenheitstraße 6, 28359 Bremen, Germany
Email: irene.kruse@nbi.ku.dk

Abstract

We provide a detailed analysis of convectively generated cold pools (CPs) over flat midlatitude land, combining ten-year high-frequency time series of measurements at several heights available from the 213-m tower observatory at Cabauw, the Netherlands, with a collocated 2D radar rainfall dataset. This combination of data allows us to relate observations of the CP's temporal and vertical structure to the properties of each CP's parent rain cell, which we identify by rain-cell tracking. Using a new detection method, based on the anomalies of both the vertically averaged wind and the temperature, we monitor the arrival and passing of 189 CPs during ten summers (2010–2019). The time series show a clear signature of vortex-like motion along the leading CP edge in the vertical and horizontal wind measurements. The arrival of CP gust fronts is

Kruse, Jan O. Haerter, and Meyer (2021) structure

Data

213-m tower observatory at Cabauw, Netherlands

→ 1-min averaged T, T_{dp}, **V** from 10, 20, 40, 80, 140, 200 m (60, 180 m in 2019)

collocated 2D radar rainfall dataset

→ 5 min and 1 km $\times$ 1 km resolution from KNMI radars in Herwijnen and Helder

10 years data of summers (May-September) 2010-2019

→ 189 Cold pool events to analyze

Schematic of convection and CP generation (Jeevanjee 2016)

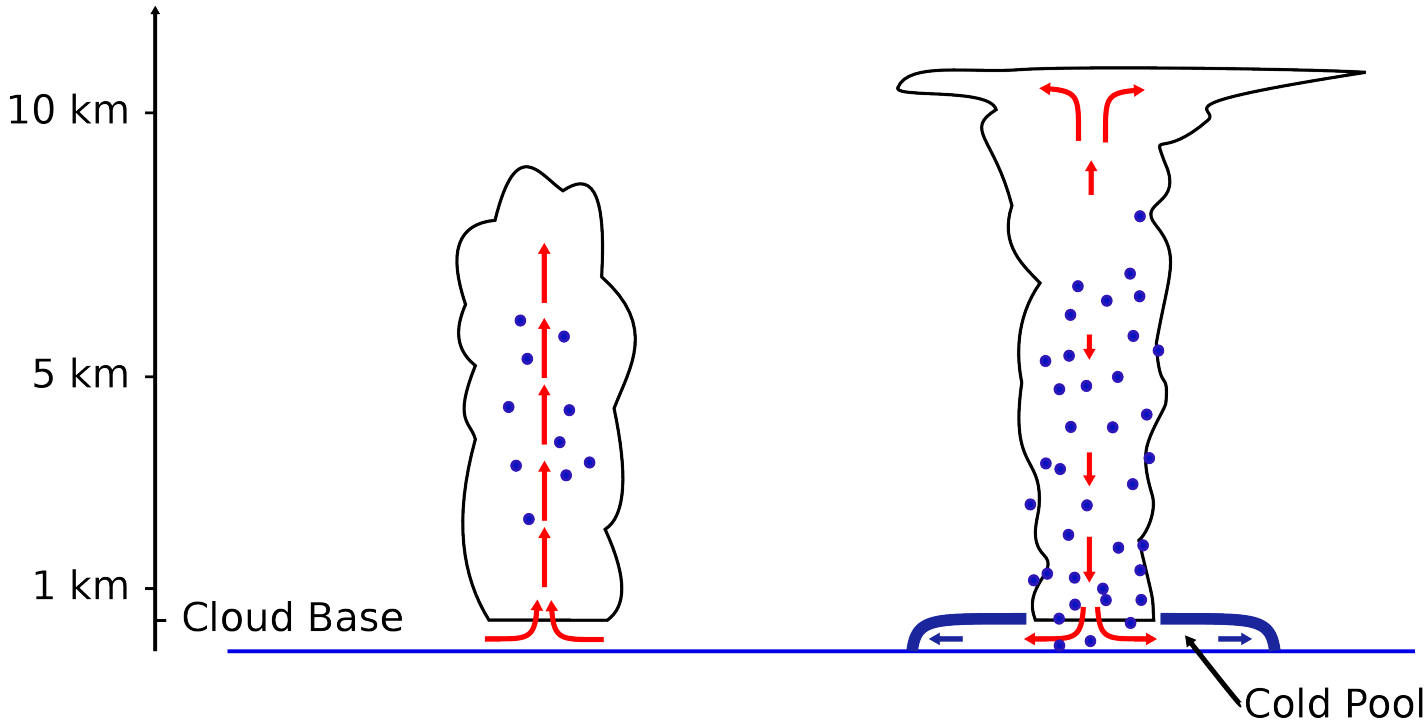

Figure 1.1: Schematic of convection and cold pool generation. **Left**: As a cloud grows, water condenses and is lofted up along with the rising air (red arrows). **Right**: As the cloud mature some of the condensed water begins to fall as rain. Some of this rain evaporates on the way down, creating negatively buoyant air which begins to descend (red arrows). When this air reaches the ground it slumps down and spreads out, forming a cold pool. Figure courtesy Wolfgang Langhans.

Algorithm for the detection of CP from tower measurements

following Szoeke et al. (2017) for T

0. smooth T (11 min moving average)
1. T_i is a T_{min} if $T_i < T_j$ for $j \in -20, \ldots, 0$
2. CP consist of consecutive T_{min} with a $T_{min,\,first}$ and $T_{min,\,last}$ (+0.5 K fluctuation are allowed)
3. T_i is T_{max} if $T_i \geq T_j$ for $j \in -10, \ldots, 0$ with $T_0 = T_{min,\,first}$
4. $\delta T = T_{max} - T_{min,\,last}$
5. Δt is the time difference between $T_{min,\,first}$ and $T_{min,\,last}$

$\rightarrow$ CP detection if $\delta T > 1.5$ K and $\Delta t \leq 60$ min

$\rightarrow$ T_{drop} equates δT for non-smoothed T

Algorithm for the detection of CP from tower measurements

novel criterion for **V**

1. smooth **V** (2 h moving average) and subtract it from **V**
2. smooth over height by averaging series over 6 heights

$\rightarrow$ height-averaged horizontal wind anomalies: Δu

3. Δu_{max} is maximum of Δu of a as CP time series (from T criterion) between 10min before $T_{min,\,first}$ and $T_{min,\,last}$

$\rightarrow$ confirm CP detection if $\Delta u_{max} > 4\sigma$, where σ is the standard deviations of the daily Δu time series

Example August 27, 2019

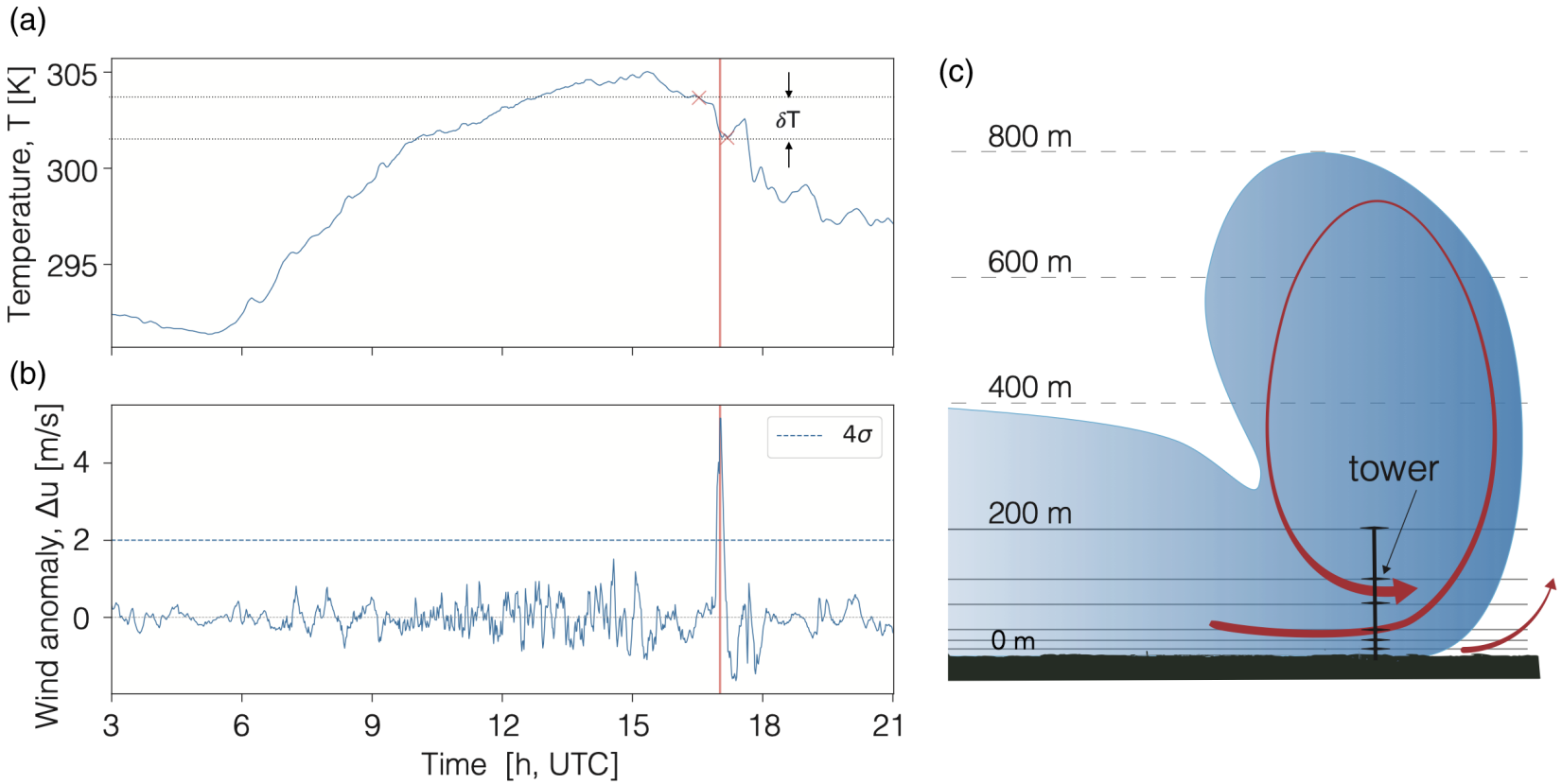

FIGURE 1 Exemplifying cold pool detection by two-step criterion. (a) Daily time series of temperature, measured at the 10 m level at 1-min temporal resolution and smoothed with an 11-min centered window. The red symbols and two horizontal lines mark the initial temperature drop δt of a detected CP event. (b) Horizontal wind anomaly averaged over all tower heights (Section 2.2) measured at 1-min temporal resolution. The anomaly is computed with respect to a 2-hr centered running temporal average. The horizontal dashed blue line indicates four standard deviations from the daily mean horizontal wind anomaly, exceedance of which is used as a criterion for the detection of strong wind anomalies. (c) Sketch of a cold pool (blue shaded area) crossing the Cabauw tower. The red arrows indicate the propagation velocity and internal circulation of the cold pool, together composing the measured horizontal wind anomaly. The levels of temperature and horizontal wind measurements (10, 20, 40, 80, 140, and 200 m) are indicated by solid horizontal black lines [Colour figure can be viewed at wileyonlinelibrary.com]

Attribution of a rain cell from radar data

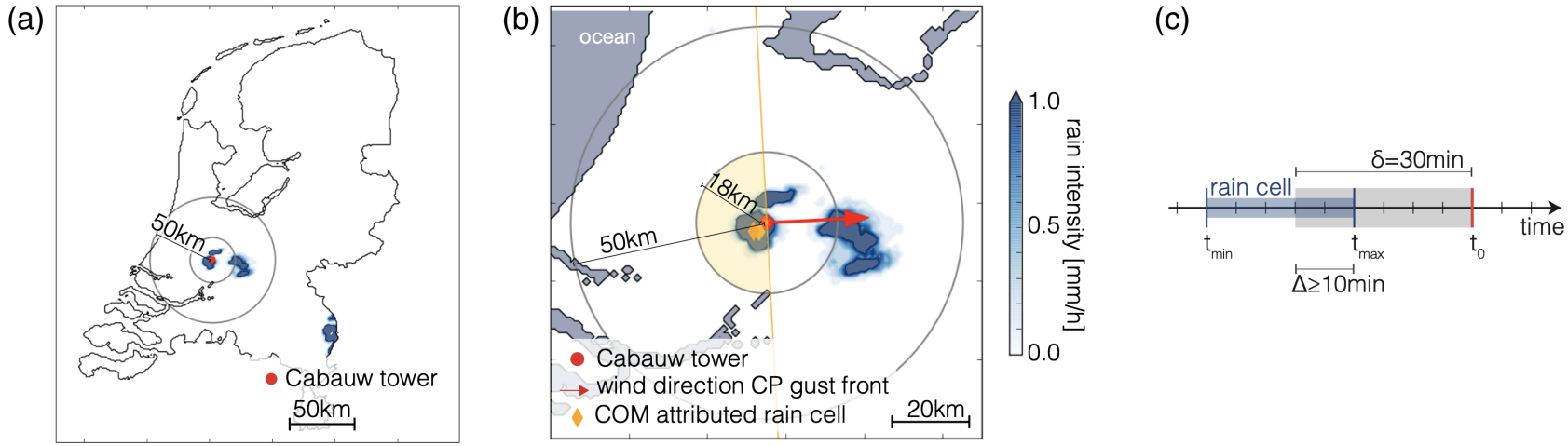

FIGURE 2 Schematic of rain cell attribution algorithm. (a) Overview of radar data domain with the location of the Cabauw tower marked. The black contour line marks the political boundary of the Netherlands. (b) Schematic of geometrical requirements on the rain cell position during $t \in [t_0 - \delta \ \min(t_0, t_{\min})]$ based on the wind direction of the detected CP gust front at time t_0. Only rain cells within the yellow half-circle are accepted. (c) Schematic of requirement on temporal overlap of rain cells that exist in the time window $t \in [t_{\min}, t_{\max}]$ [Colour figure can be viewed at wileyonlinelibrary.com]

- Iterative Raincell Tracking by Moseley, Berg, and Jan O Haerter (2013)
- Attribution of the closest rain cell (at least 10 min lasting) from the previous 30 min before the CP located in front of the tower (with respect to the wind direction)

$\rightarrow$ 116 of 189 CPs are attributed to unique rain cell

Example August 27, 2019

FIGURE 3 Cold pool developing around Herwijnen radar tower. The Herwijnen tower is marked as an "x" in each figure. Radar reflectivity (left column) and Doppler radial velocity (right column) were recorded on August 27, 2019 in 10-min steps from 16:40 to 17:00 as marked in panels (a)–(c), respectively. The gust front is clearly seen as a ring of low reflectivity values spreading around the largest rain event. This ring corresponds to positive radial velocities. We note that the measurements shown are taken at an elevation angle of 1.20°. In (a), the gust front is observed at approximately 200 m asl, whereas in (c) the observed height is approximately 400 m asl [Colour figure can be viewed at wileyonlinelibrary.com]

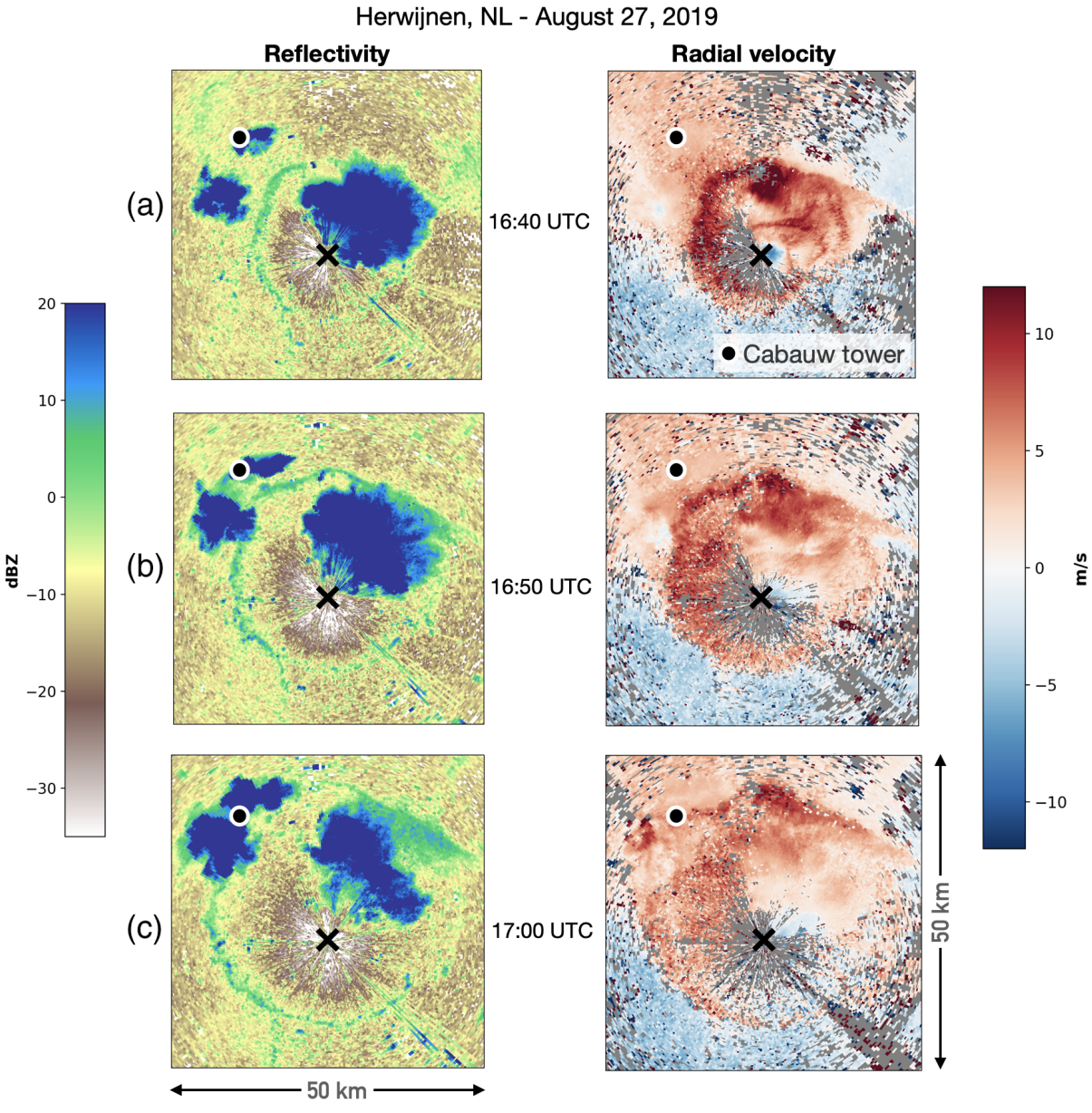

CP composite time series for V_h and T

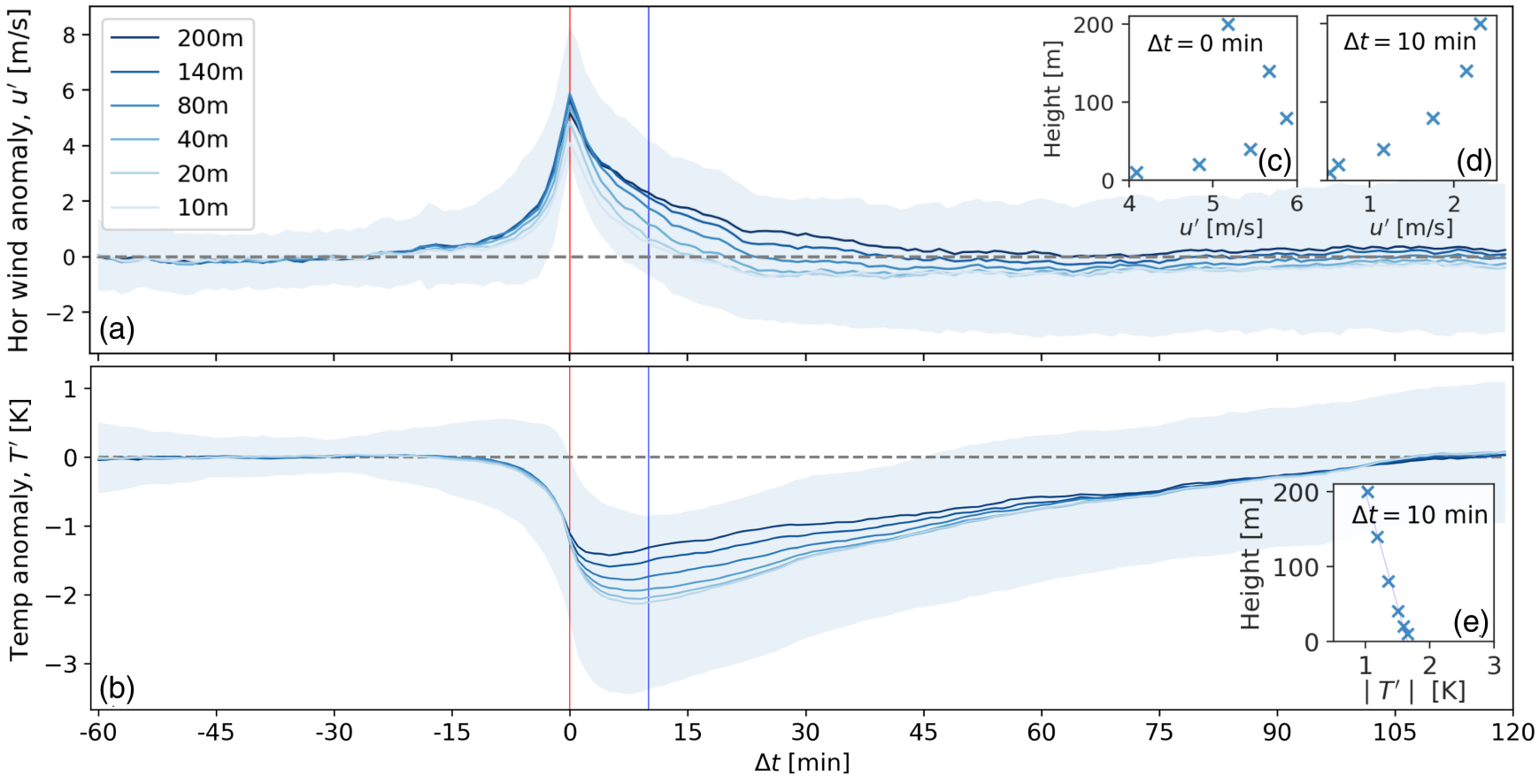

FIGURE 4 Composite time series of (a) horizontal wind anomaly u' and (b) temperature anomaly T'. These composites include 189 CPs detected in the summers 2010–2019. Blue lines show the ensemble mean; blue shaded areas show the standard deviation, computed from the CP ensemble, indicating the ensemble spread between the different CPs at each given time, and computed at the height of the strongest signal for each variable (80 m for the horizontal wind, 10 m for the temperature). Vertical lines highlight times $\Delta t = 0$ min (red) and $\Delta t = 10$ min (blue). Insets show (c) u' at the heights measured at the tower at $\Delta t = 0$ min; (d) analogous to (c) but at $\Delta t = 10$ min; (e) T' at the heights measured at the tower at $\Delta t = 10$ min, with linear fit used to estimate CP height (intercept: 503.8, slope: −304.7) [Colour figure can be viewed at wileyonlinelibrary.com]

CP composite time series for w and WVC (only 2019)

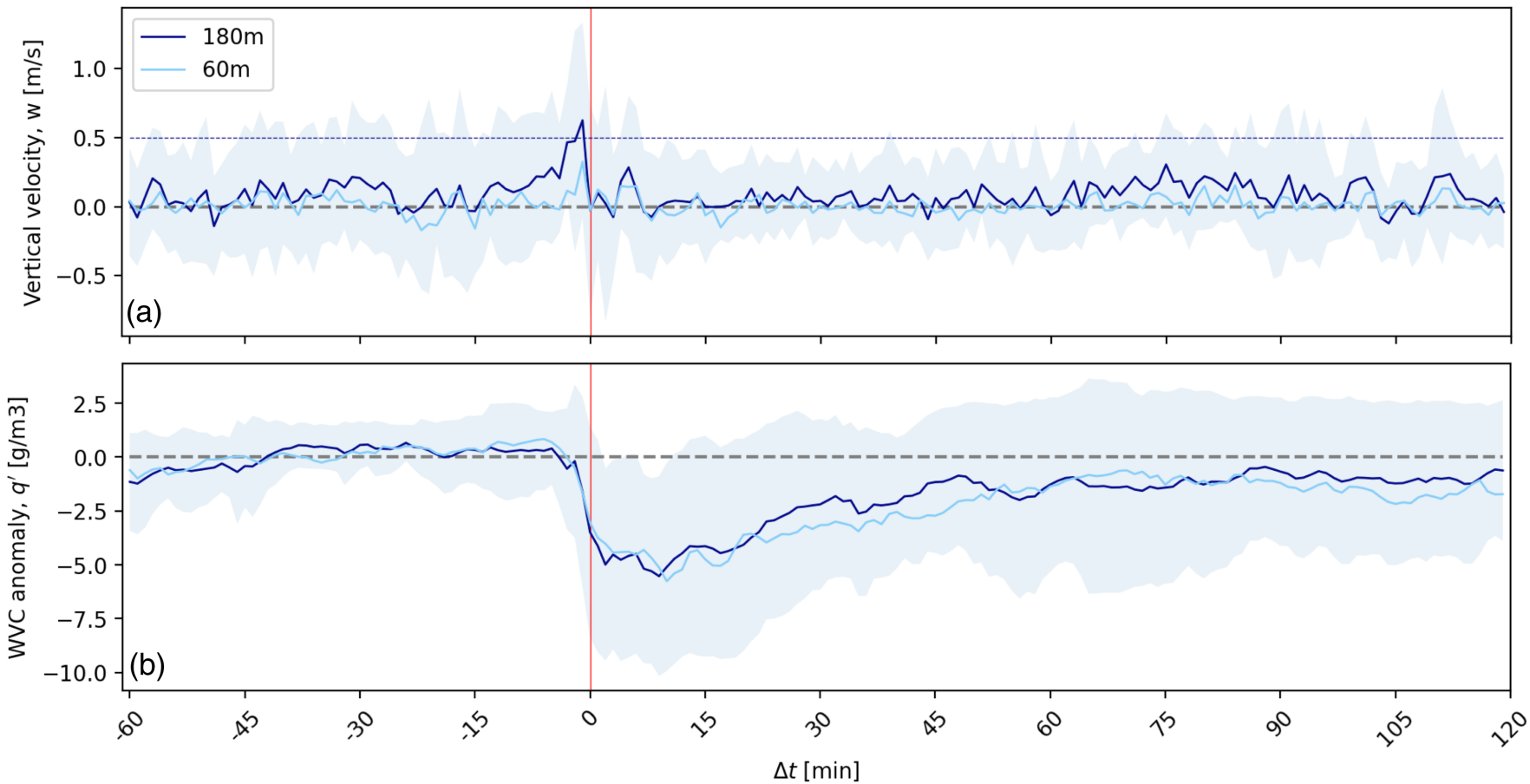

FIGURE 5 Composite time series of (a) vertical velocity and (b) water-vapor concentration (WVC) anomaly. These composites include 18 CPs detected in the summer of 2019. Blue shaded areas in each panel show the standard deviation, computed from the CP ensembles, indicating the ensemble spread between the different CPs at a given time, and computed at the height of the strongest signal for each variable (180 m for the vertical velocity, 180 m for the WVC). The vertical red line highlights time $\Delta t = 0$ min [Colour figure can be viewed at wileyonlinelibrary.com]

Summary sketch of CP characteristics

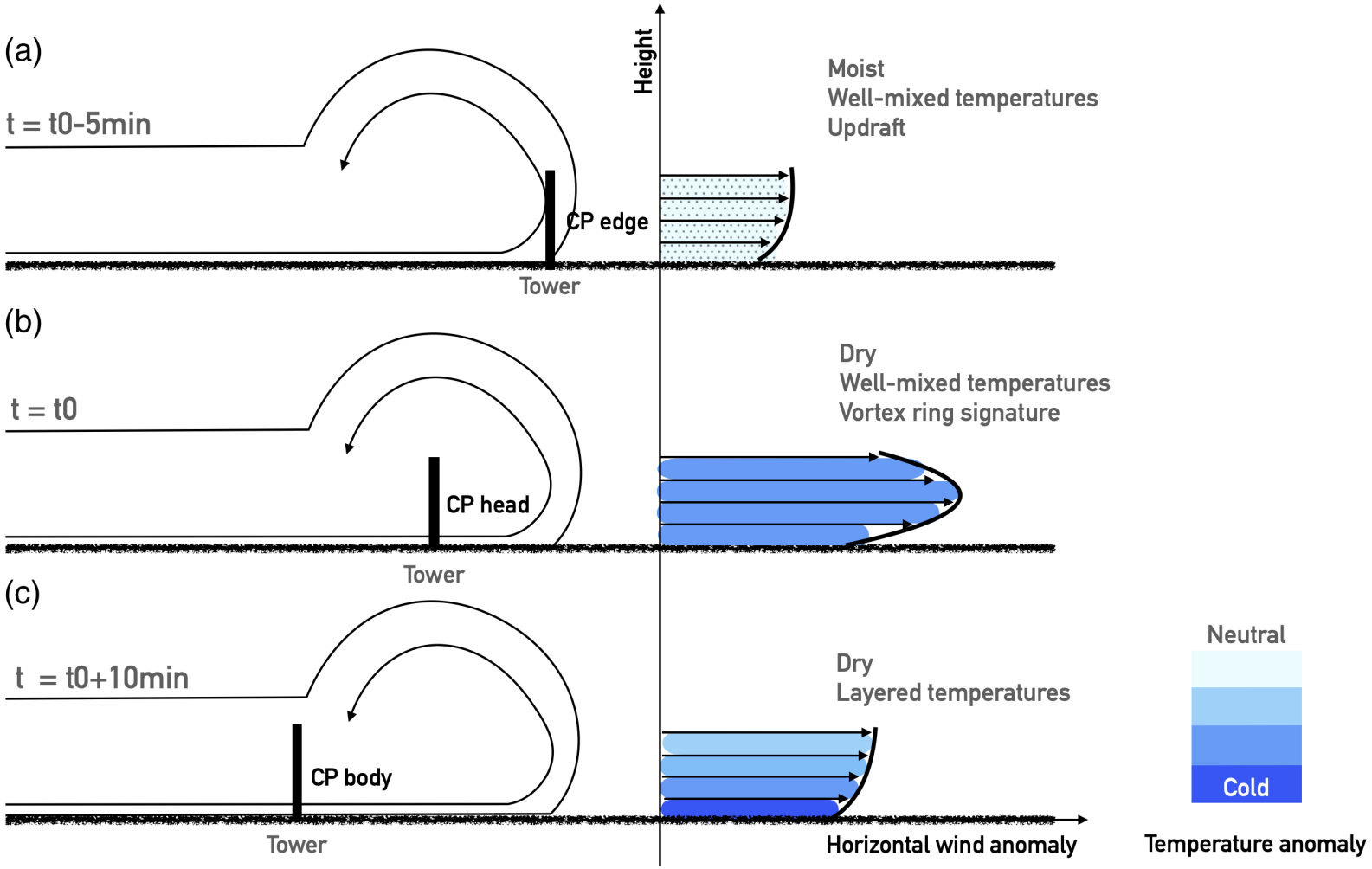

FIGURE 6 Summarizing sketch of measured CP properties. On the left is an approximate sketch of which part of the CP is being measured at the tower at a given point in time: (a) at $t = t_0 - 5$ min, the edge of the CP is being measured at the tower; (b) at $t = t_0$, the head of the CP; (c) at $t = t_0 + 10$ min, the body of the CP. On the right, a depiction of the measured CP properties corresponding to each part of the CP measured at its lowest 200 m is given: the edge of the CP shows moist, well-mixed air, along with an updraft; the head of the CP shows dry, colder, well-mixed air, and the signature of a vortex ring is reflected in the horizontal wind anomaly; the body of the CP shows dry air and a layered temperature anomaly, with the largest cold anomaly within the bottom layers [Colour figure can be viewed at wileyonlinelibrary.com]

CP strength

Consider CP propagation u ($\approx \Delta u_{\max}$) similar to density current

$$u = k\sqrt{gH\frac{\Delta T}{T_0}}, \text{with} \tag{1}$$

$k \approx 0.7$ internal Froude number,
g Gravity acceleration,
H CP height (estimated to $H \approx a = 478\,\text{m}$, sensitive to k),
ΔT temperature difference CP to environment ($\approx T_{drop}$),
T_0 environment temperature (10 m tower mean)

CP strength

theoretical fit (red), linear fit (green)

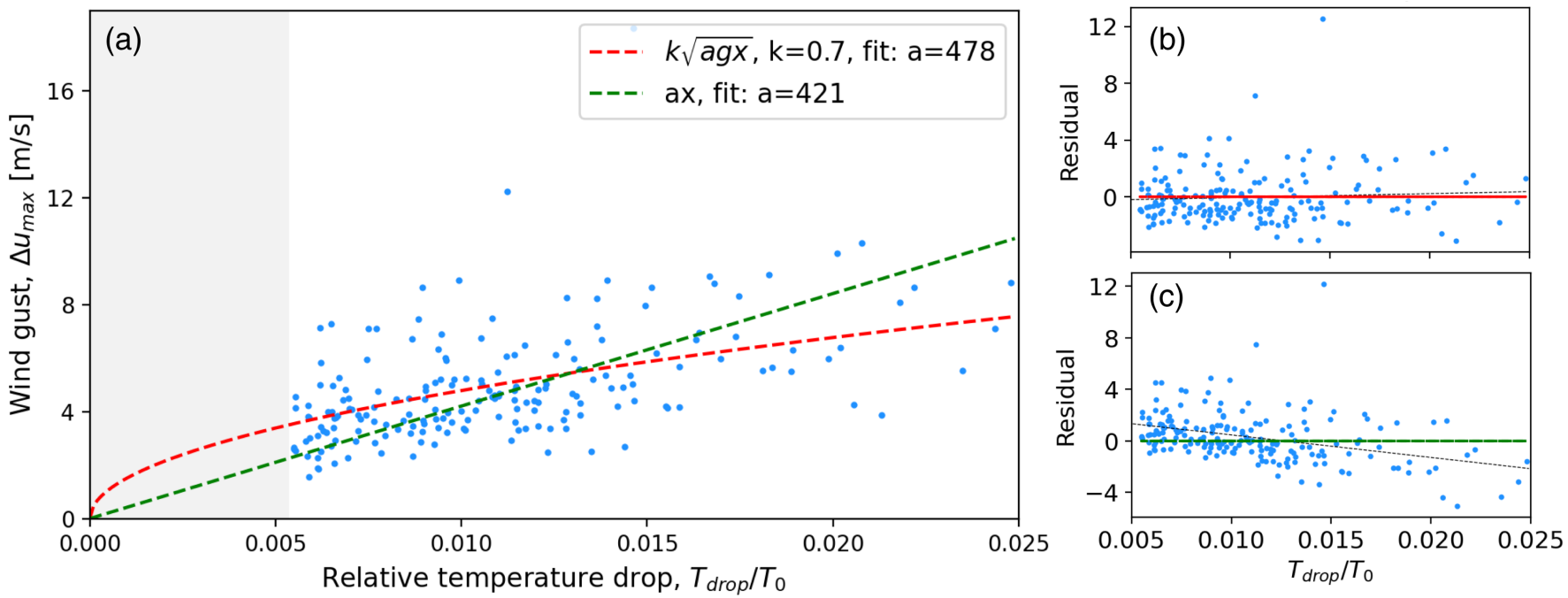

FIGURE 7 Cold pool property relationship compared with the theoretical model. (a) Gust front strength $\Delta u_{\max}$ versus relative temperature drop T_{drop}/T_0 for all CPs detected during 2010–2019. Considering Equation 3, the fitting constant a in the square-root fit can be understood as an estimate of the CP height. In the fitting functions, x corresponds to the values on the x-axis. (b) Residuals from square-root fit (Equation 3), trend shown as a thin dotted black line. Approximately symmetric spread around zero (red line). (c) Same as (b), but for linear fit. Systematic tendency with an underestimation (overestimation) of $\Delta u_{\max}$ for low (high) T_{drop}/T_0 [Colour figure can be viewed at wileyonlinelibrary.com]

CP strength: relate T_{drop} with rain cell

dew-point depression: $\widetilde{T} = \overline{T} - \overline{T}_{dp}$

spatial averaged rain intensity from radar: $< I >$

$$T_{drop} = \alpha_1 < I > + \alpha_2 \widetilde{T} + \alpha_3 < I >^2 + \alpha_4 \widetilde{T}^2 + O(3) \qquad (2)$$

TABLE 1 Fitted coefficients for the linear and nonlinear regression models (Equation 5)

	Linear regression		Nonlinear regression	
	Coeff.	Std. error	Coeff.	Std. error
α_1 [K·hr mm^{-1}]	0.25	0.03	0.44	0.09
α_2 [–]	0.40	0.03	0.51	0.08
α_3 [K·hr^2·mm^{-2}]			−0.020	0.007
α_4 [K^{-1}]			−0.021	0.007
R-squared (uncentered)	0.89		0.92	

Note: α_1 and α_2 represent the coefficients of the terms linear in rain intensity and temperature, respectively, whereas α_3 and α_4 represent the coefficients of the terms quadratic in rain intensity and temperature, respectively.

CP is 1 K colder (due to lin fit)

→ from 4 mm/h more rain

→ from 2.5 K larger dew point depression

Conclusion

→ The patterns in the horizontal and vertical wind measurements confirm the existence of a vortex ring in the CP head.

→ The detected CPs show weak or absent moisture rings, while the CP interior shows a negative moisture anomaly.

→ A simple model consisting of a multivariate linear combination of pre-event dew-point depression and area-averaged rainfall intensity allows a prediction of the generated CP's strength

Review

+ nice CP statistics
+ comprehensible approach for CP detection

- missing evaluation of $\Delta u_{\max} \sim \frac{\Delta T}{T_0}$ relation
- why should a $(= H)$ be always equal?
- $< I >$ is taken at what time?
- working 'prediction' for given CP events but what is about dew-point depressions without CP?

+ well applicable and novel recipe for CP detection

References

Jeevanjee, Nadir (2016). “Cold Pools, Effective Buoyancy, and Atmospheric Convection”. Dissertation. University of California, Berkeley, USA.

Kruse, Irene L., Jan O. Haerter, and Bettina Meyer (Dec. 2021). “Cold pools over the Netherlands: A statistical study from tower and radar observations”. In: *Quarterly Journal of the Royal Meteorological Society*. DOI: *10.1002/qj.4223*. URL: *https://doi.org/10.1002/qj.4223*.

Moseley, Christopher, Peter Berg, and Jan O Haerter (Dec. 2013). “Probing the precipitation life cycle by iterative rain cell tracking”. en. In: *J. Geophys. Res.* 118.24, pp. 13, 361–13, 370.

Szoeke, Simon P. de et al. (Apr. 2017). “Cold Pools and Their Influence on the Tropical Marine Boundary Layer”. In: *Journal of the Atmospheric Sciences* 74.4, pp. 1149–1168. DOI: *10.1175/jas-d-16-0264.1*. URL: *https://doi.org/10.1175/jas-d-16-0264.1*.